Supporting Information

C_2H_2 Selective Hydrogenation over the M@Pd and M@Cu(M=Au, Ag, Cu and Pd) Core-Shell Nanocluster Catalysts: The Effects of Composition and Nanocluster Size on Catalytic Activity and Selectivity

Riguang Zhang[a,b], Mifeng Xue[a], Baojun Wang[a,*], Lixia Ling[a], Maohong Fan[b,c,d,*]

[a] *Key Laboratory of Coal Science and Technology of Ministry of Education and Shanxi Province, Taiyuan University of Technology, Taiyuan 030024, Shanxi, P.R. China*

[b] *Department of Chemical Engineering and Department of Petroleum Engineering, University of Wyoming, Laramie, WY 82071, USA*

[c] *School of Civil and Environmental Engineering, Georgia Institute of Technology, Atlanta, GA 30332 USA*

[d] *School of Energy Resources, University of Wyoming, Laramie, WY 82071, USA*

1. The choice of the functional (PBE) and the core treatment parameter (ECP)

In this study, for the type choice of DFT exchange-correlation potential used in the calculation, nowadays, the GGA-PW91[1] and GGA-PBE[2] functional have been widely employed in the calculation system of metal catalyst. The PW91 reduces to the second-order gradient expansion for density variations that are either slowly varying or small, it describes the linear response of the density of a uniform electron gasless satisfactorily than does local spin density (LSD); however, the PBE improves upon the local spin density (LSD) description of atoms, molecules, and solid. Furthermore, in comparison with the PW91, the GGA-PBE enhanced the accurate description of the linear response of the uniform electron gas, correct behavior under uniform scaling, and a smoother

*Corresponding author at: wangbaojun@tyut.edu.cn; wbj@tyut.edu.cn (Baojun Wang) and mfan@uwyo.edu (Maohong Fan)

potential. Further, the activation free energy of C_2H_4 hydrogenation to C_2H_5 over $Au@Pd_{12}$ and $Ag@Pd_{12}$ clusters has been calculated using the GGA-PW91 and GGA-PBE functional, respectively. As listed in Table S1, the activation free energy of C_2H_4 hydrogenation over $Au@Pd_{12}$ and $Ag@Pd_{12}$ clusters through GGA-PBE functional are 113.3 and 113.0 kJ·mol^{-1}, respectively, which are closed to the activation free energy through GGA-PW91 (116.8 and 114.4 kJ·mol^{-1}, respectively). Thus, the calculation results using GGA-PBE functional is reliable for the qualitative evaluation of C_2H_4 selectivity over different M@Pd and M@Cu core-shell catalysts.

Table S1 The activation free energy (kJ·mol^{-1}) of C_2H_4 hydrogenation over $Au@Pd_{12}$ and $Ag@Pd_{12}$ clusters through different functional.

Clusters	GGA-PBE	GGA-PW91
$Au@Pd_{12}$	113.3	116.8
$Ag@Pd_{12}$	113.0	114.4

On the other hand, the effective core potentials (ECP) employed in the computations is the core treatment parameter, which controls how electrons in the lowest lying atomic orbitals are treated. Four types of treatments of core electrons[3-5] including in All Electron, Effective Core Potential, All Electron Relativistic, or DFT Semi-core Pseudopots are available in DMol^3 program. The default setting, All Electron, treats these in the same manner as valence electrons, and is appropriate for atoms up to about atomic number 36 (Kr). However, with heavier elements, relativistic effects become important in the core electrons. One method of incorporating these effects is to use the All Electron Relativistic option. As the name implies, the core electrons are still included in the calculation, but scalar relativistic effects are included.[6,7] This yields a more accurate calculation, but increases the computational cost. An alternative to all-electron calculations is to use DFT Semi-core Pseudopots[8] or Effective Core Potentials.[9,10] These replace the effects of core electrons with a simple

potential. Because the core electrons are dropped, the calculation is less computationally expensive, but because these core potentials include some degree of relativistic effects, they can be very useful approximations for heavier elements. Currently, DSPPs and ECPs are provided beginning with element number 21, Sc. For example, in our research system containing C, H, Cu, Ag, Pd and Au, if you opt to use ECPs or DSPPs, only the core electrons for Cu, Ag, Pd and Au will be replaced; C and H will be treated as in the all-electron case. Thus, the effective core potential (ECP) is used to describe the interaction between atomic core and electrons of metal in this study.

2. The stable adsorption configuration of C_2H_x(x=2-5) species

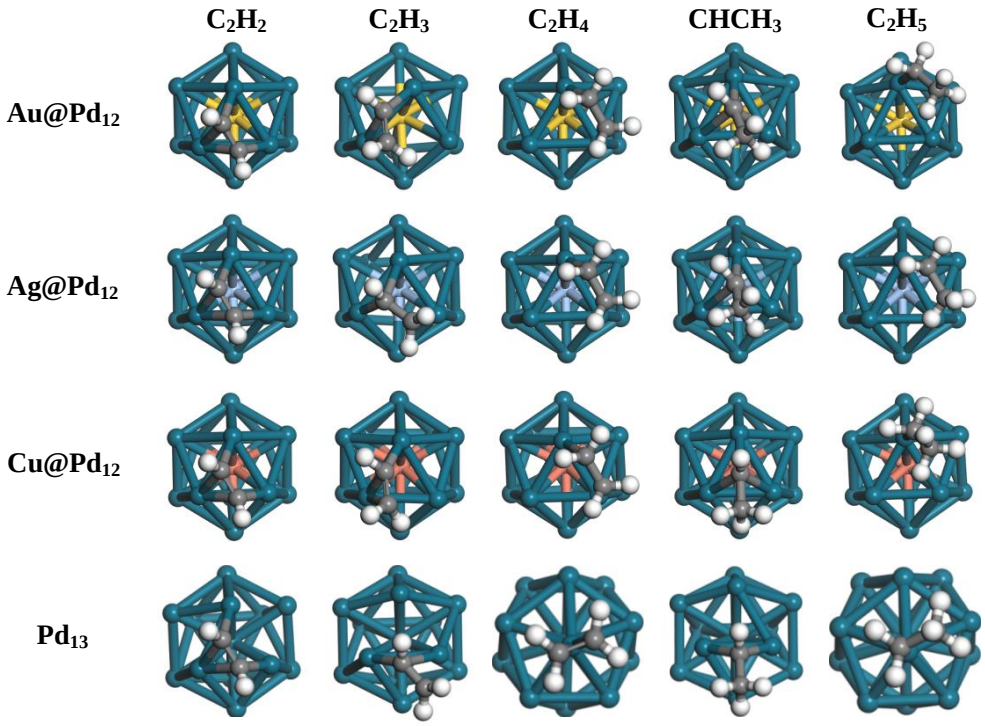

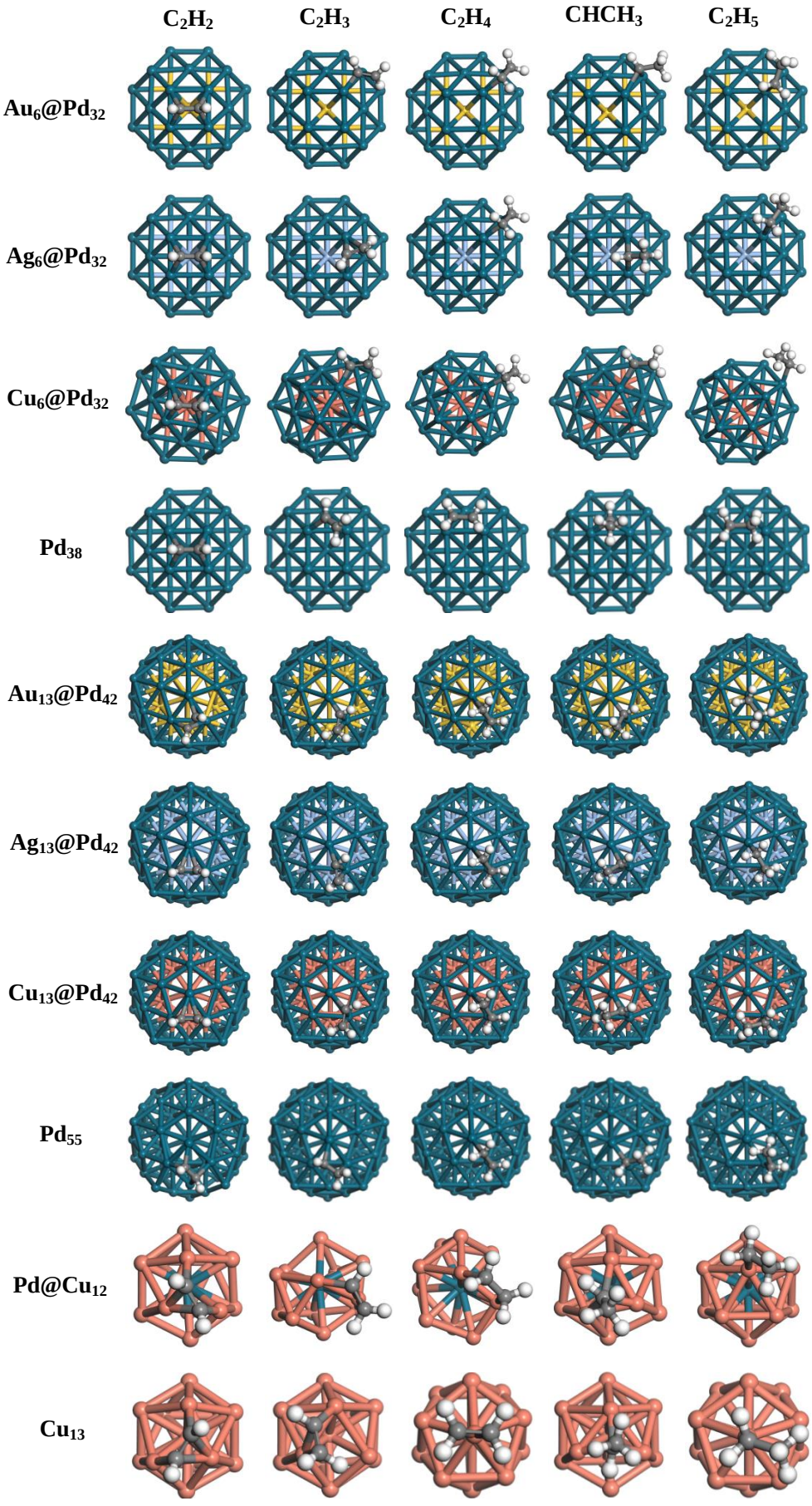
C2H2
C2H3
C2H4
CHCH3
C2H5
Au6@Pd32
Ag6@Pd32
Cu6@Pd32
Pd38
Au13@Pd42
Ag13@Pd42
Cu13@Pd42
Pd55
Pd@Cu12
Cu13

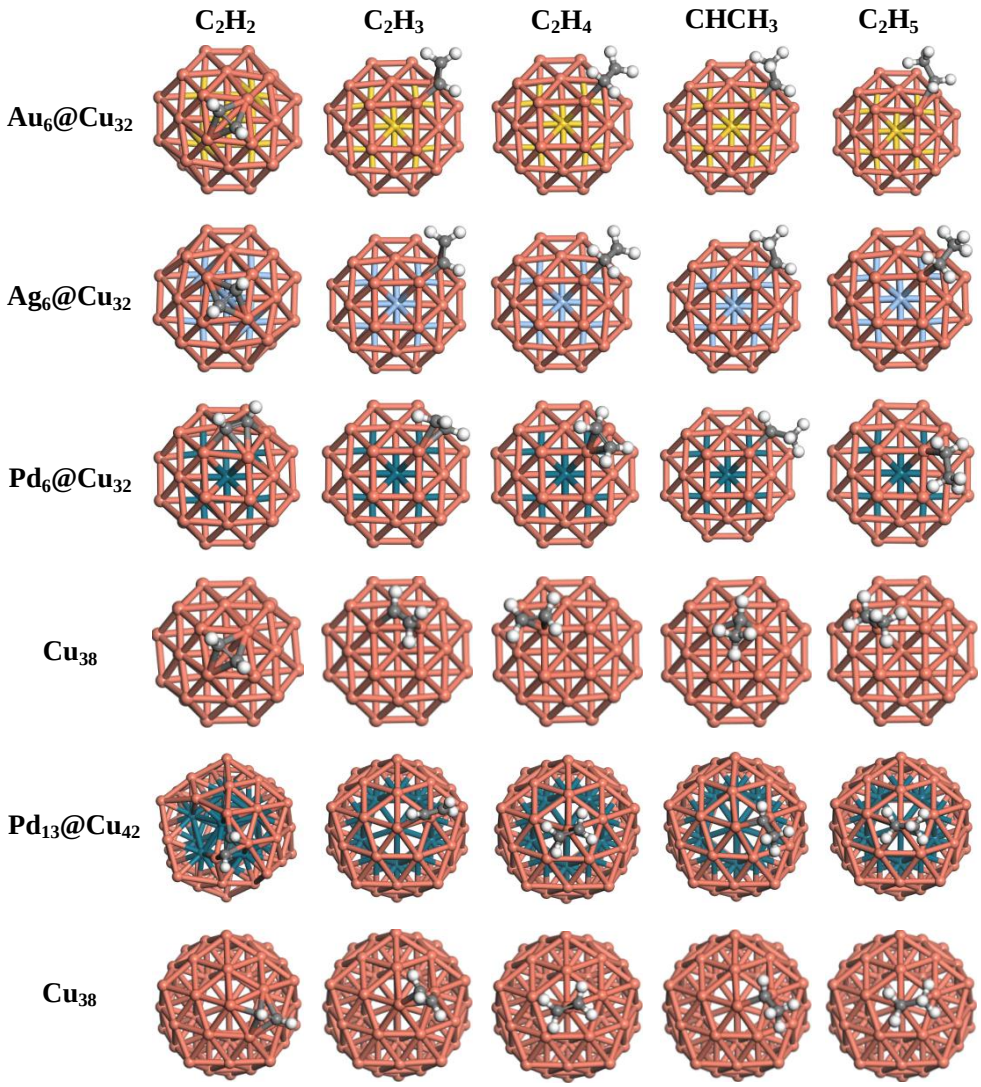

Figure S1 The most stable adsorption configurations of C_2H_2, C_2H_3, $CHCH_3$, C_2H_4 and C_2H_5 species involving in C_2H_2 selective hydrogenation over different sizes of the M@Pd (M=Au, Ag and Cu), M@Cu (M=Au, Ag and Pd) as well as the single Cu and Pd clusters.

3. The potential profiles together with the structures of initial states, transition states, final states involving in C_2H_2 selective hydrogenation over different composition and size of core-shell nanocluster with good C_2H_4 selectivity

3.1 Over different sizes of M@Pd(M=Au, Ag and Cu) nanoclusters

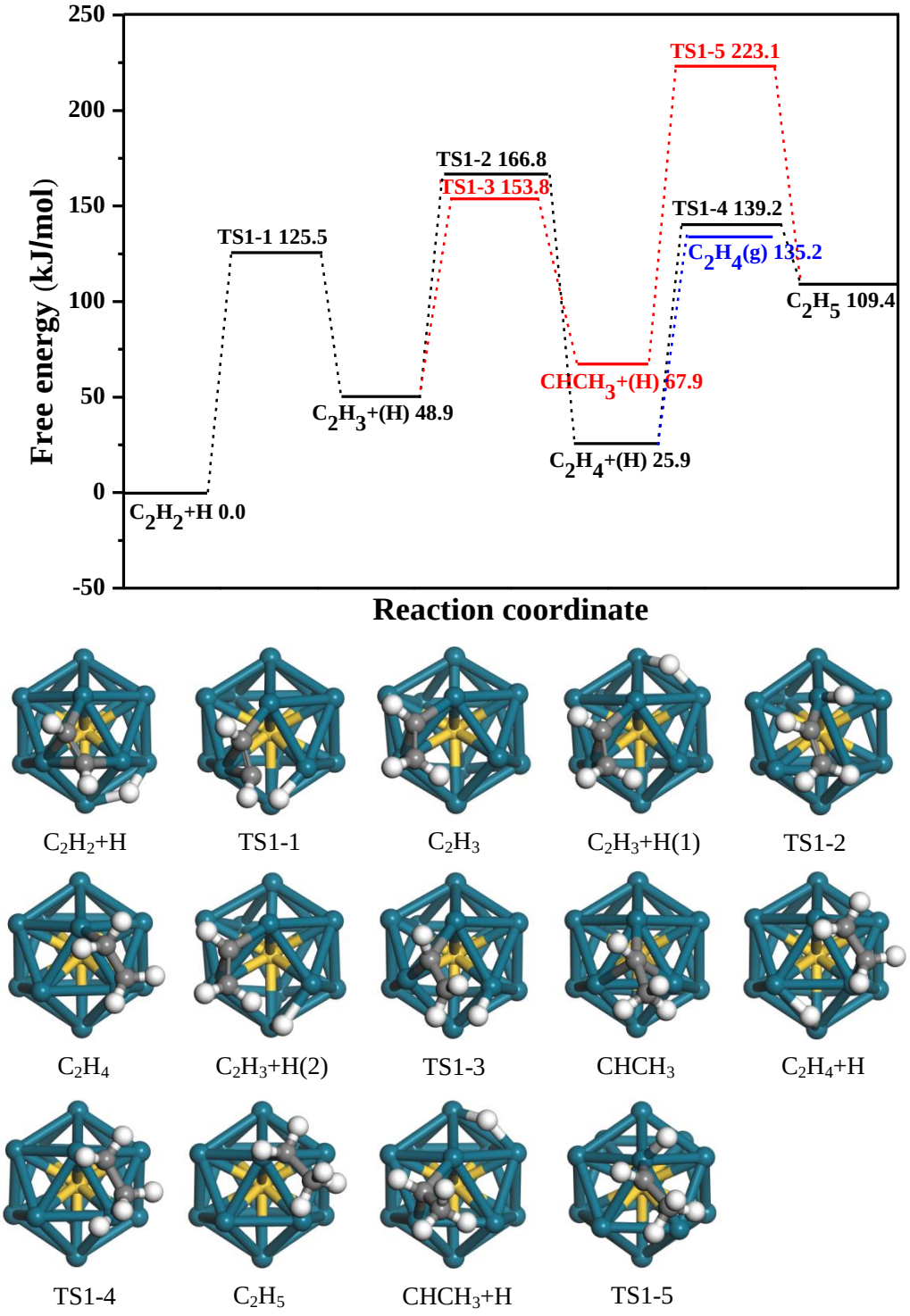

Figure S2 The structures of initial states, transition states, final states of three possible routes involving in C_2H_2 selective hydrogenation on $Au@Pd_{12}$ cluster.

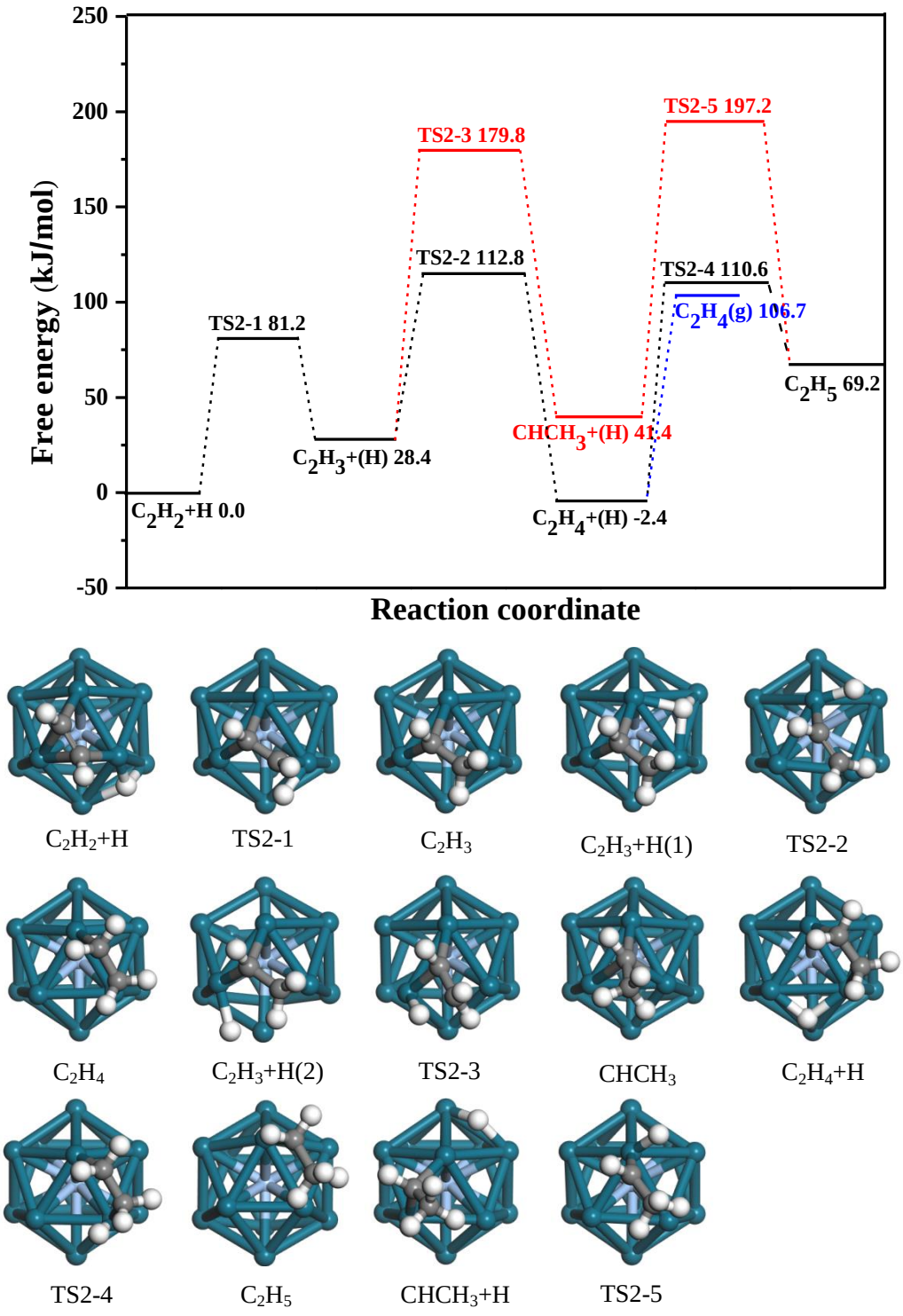

Figure S3 The structures of initial states, transition states, final states of three possible routes involving in C_2H_2 selective hydrogenation on $Ag@Pd_{12}$ cluster.

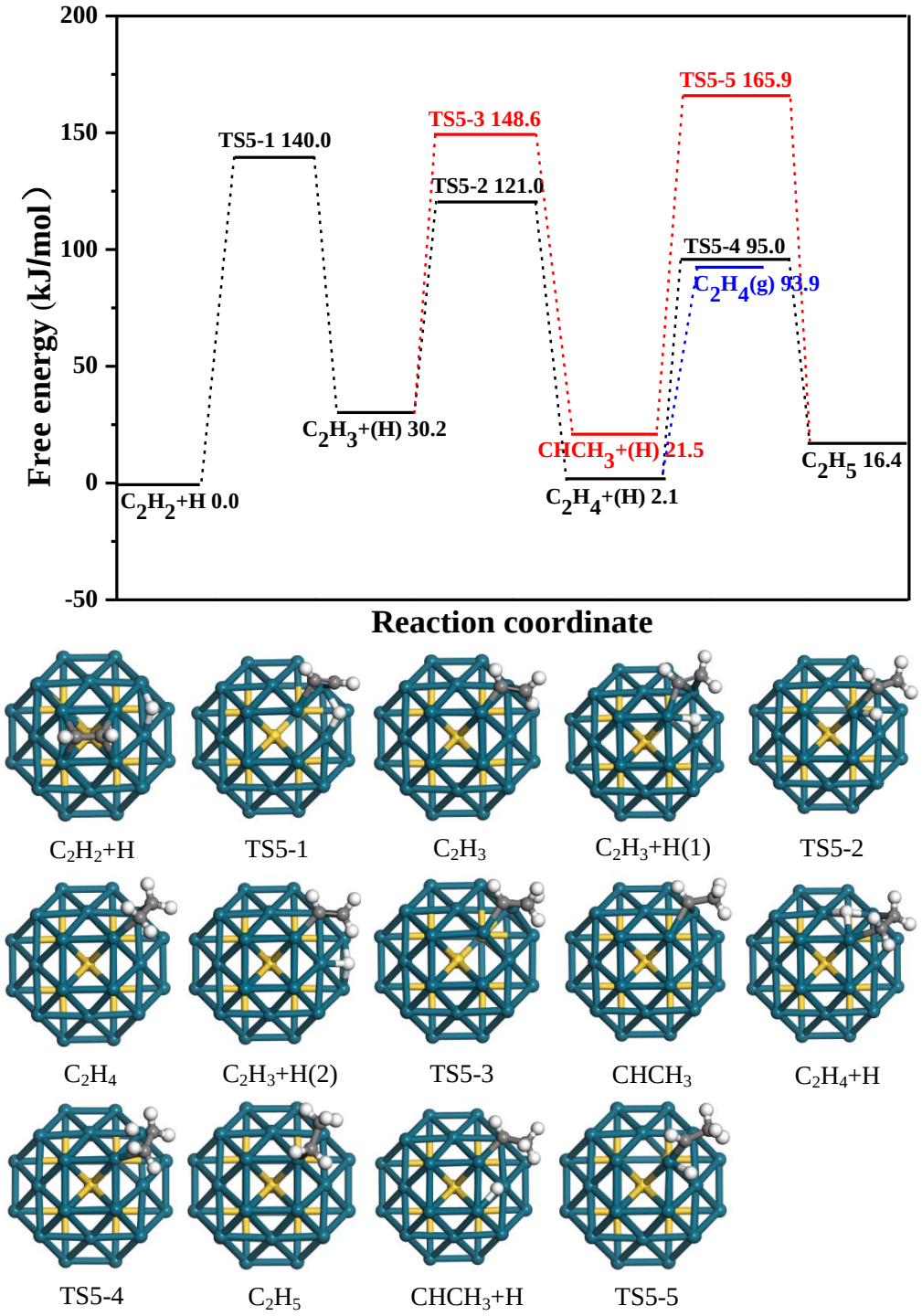

Figure S4 The structures of initial states, transition states, final states of three possible routes involving in C_2H_2 selective hydrogenation on $Au_6@Pd_{32}$ cluster.

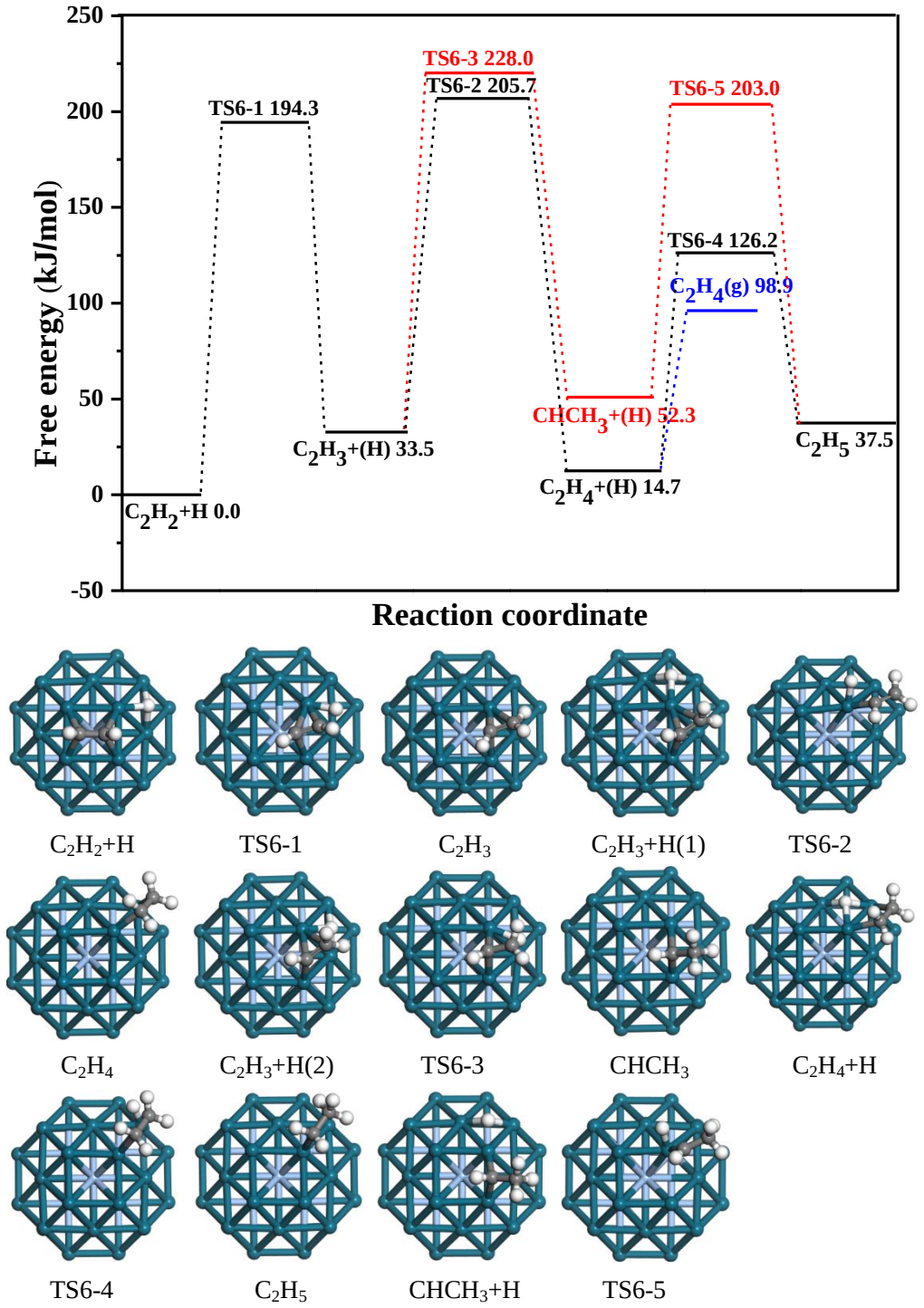

Figure S5 The structures of initial states, transition states, final states of three possible routes involving in C_2H_2 selective hydrogenation on $Ag_6@Pd_{32}$ cluster.

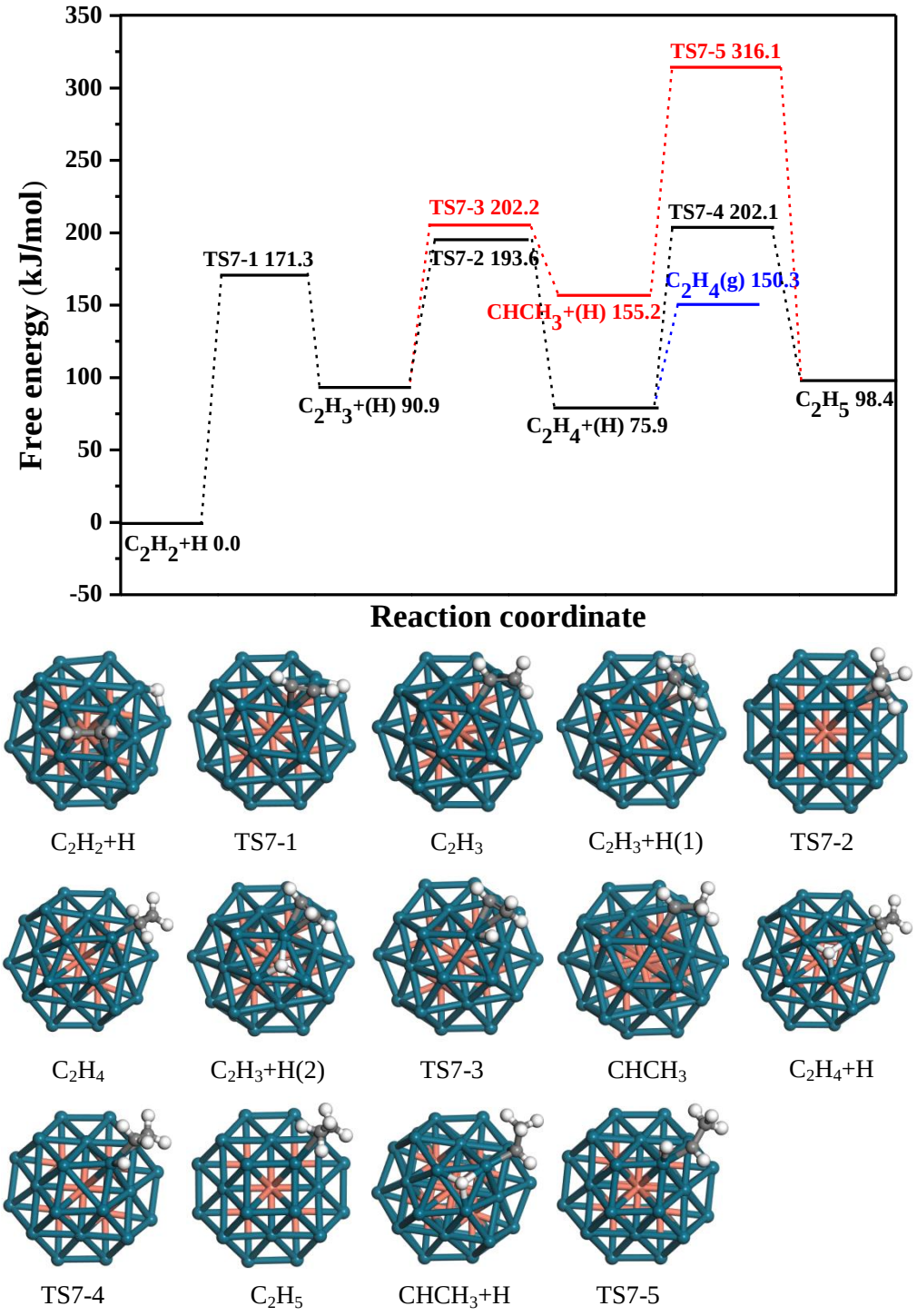

Figure S6 The structures of initial states, transition states, final states of three possible routes involving in C_2H_2 selective hydrogenation on $Cu_6@Pd_{32}$ cluster.

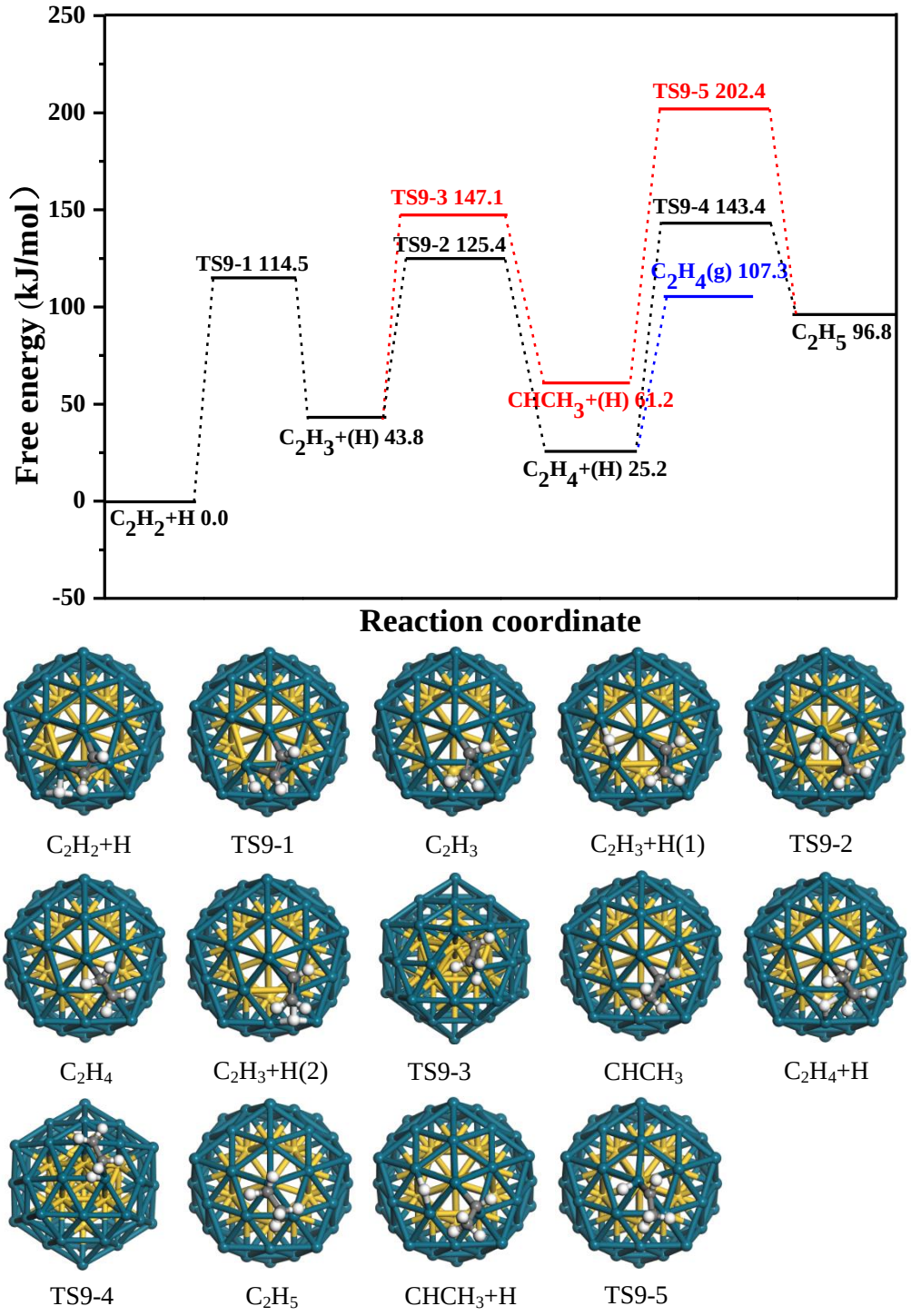

Figure S7 The structures of initial states, transition states, final states of three possible routes involving in C_2H_2 selective hydrogenation on $Au_{13}@Pd_{42}$ cluster.

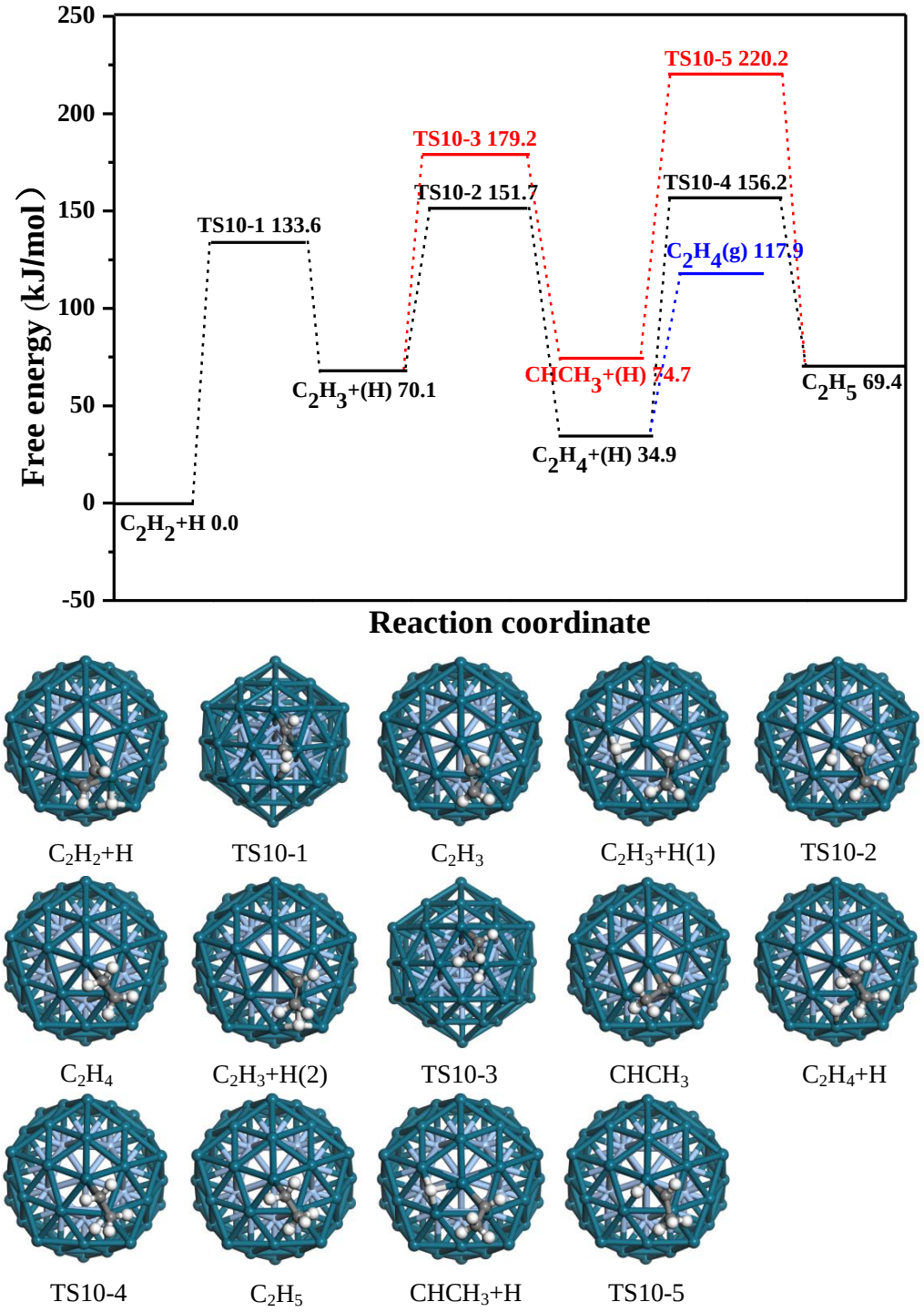

Figure S8 The structures of initial states, transition states, final states of three possible routes involving in C_2H_2 selective hydrogenation on $Ag_{13}@Pd_{42}$ cluster.

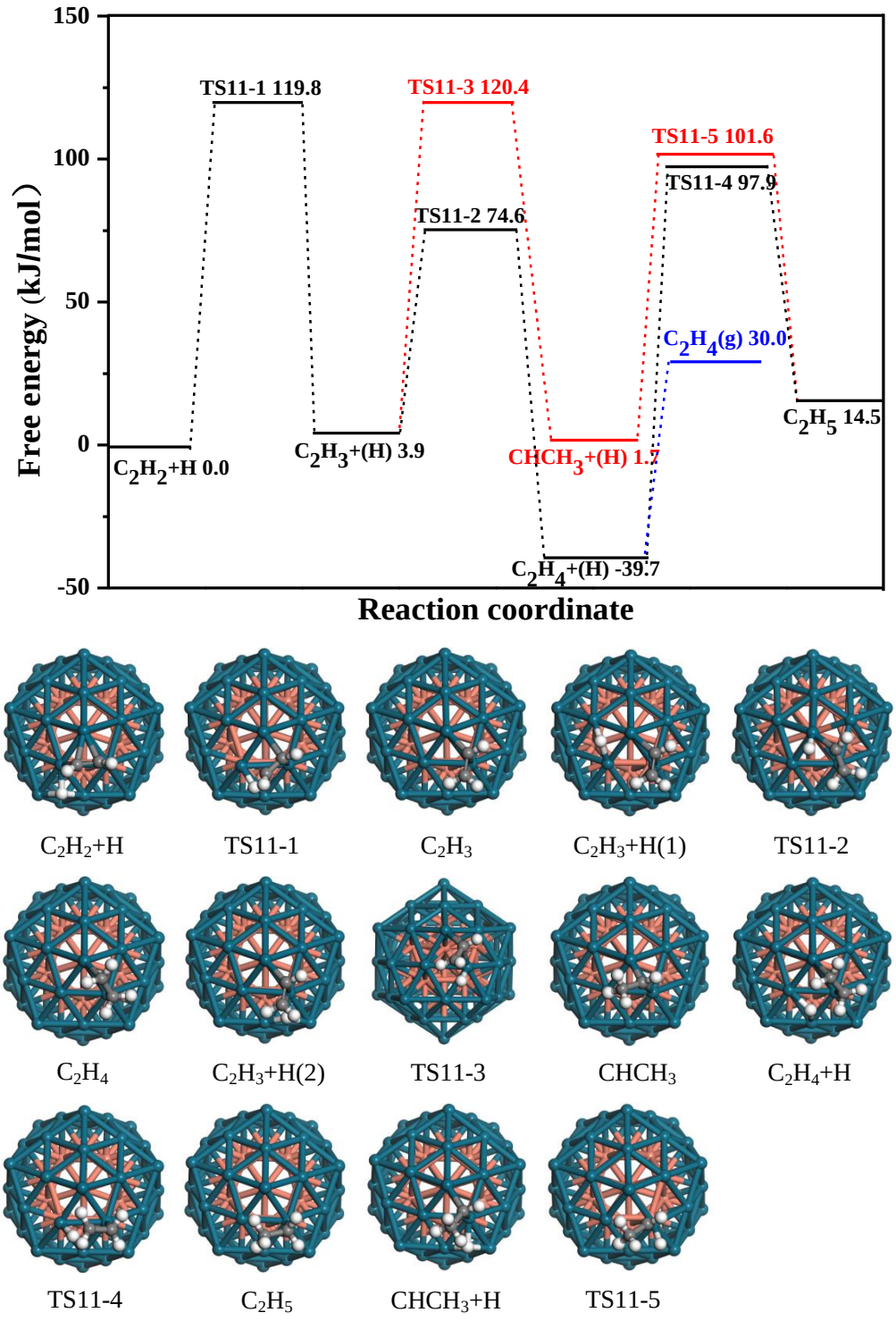

Figure S9 The structures of initial states, transition states, final states of three possible routes involving in C_2H_2 selective hydrogenation on $Cu_{13}@Pd_{42}$ cluster.

3.2 Over different sizes of M@Cu(M=Au, Ag and Pd) nanoclusters

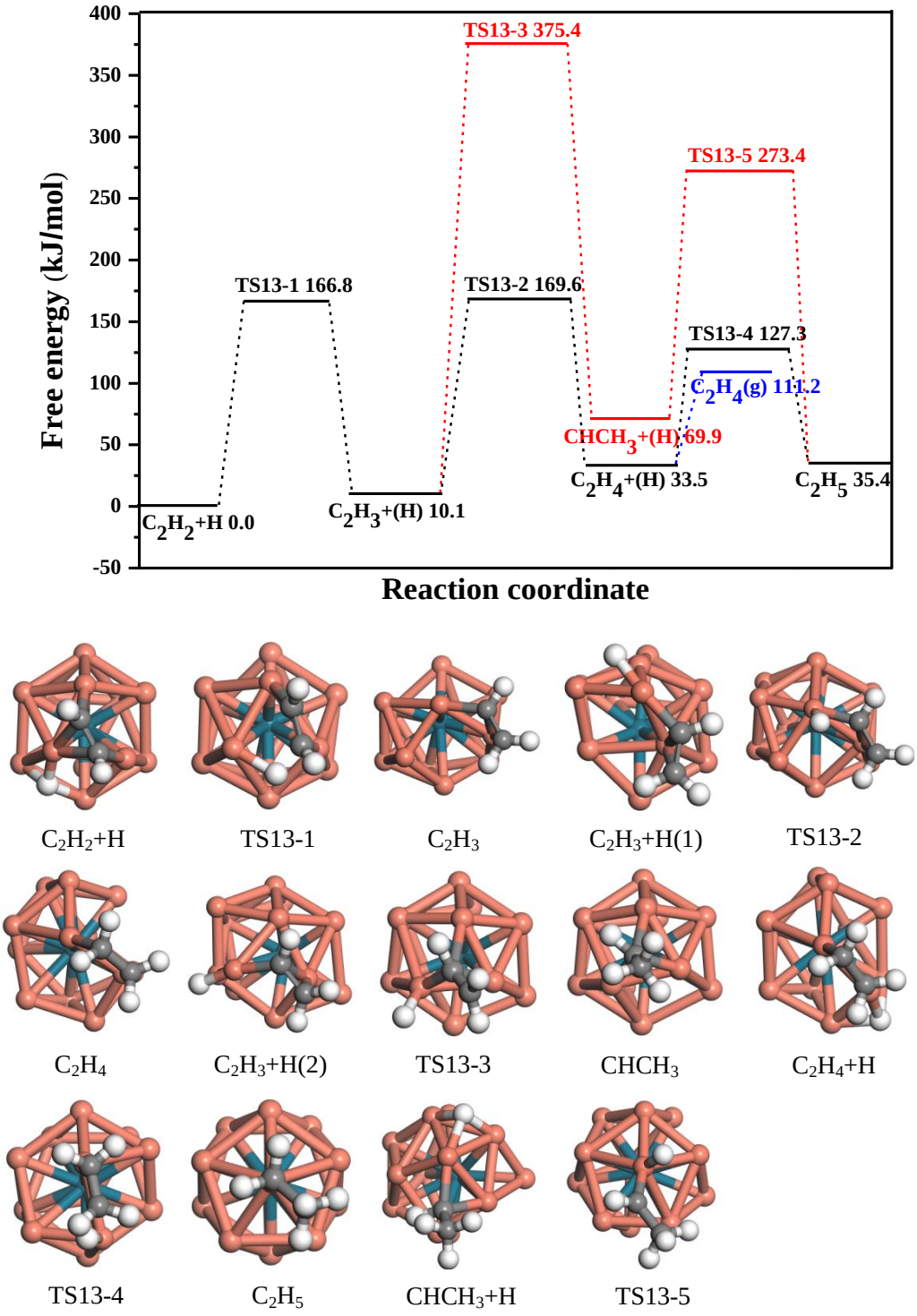

Figure S10 The structures of initial states, transition states, final states of three possible routes involving in C_2H_2 selective hydrogenation on Pd@Cu_{12} cluster.

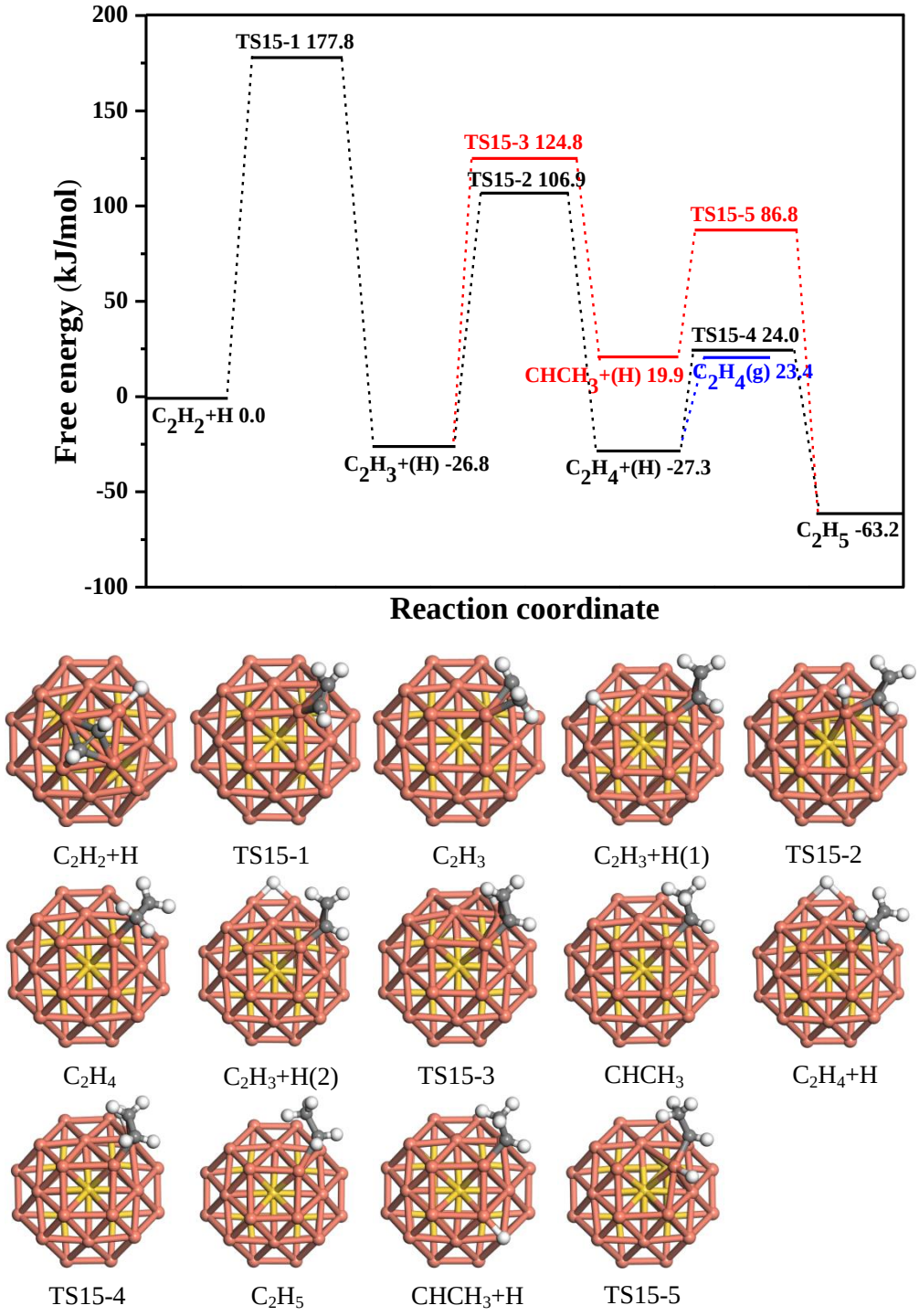

Figure S11 The structures of initial states, transition states, final states of three possible routes involving in C_2H_2 selective hydrogenation on $Au_6@Cu_{32}$ cluster.

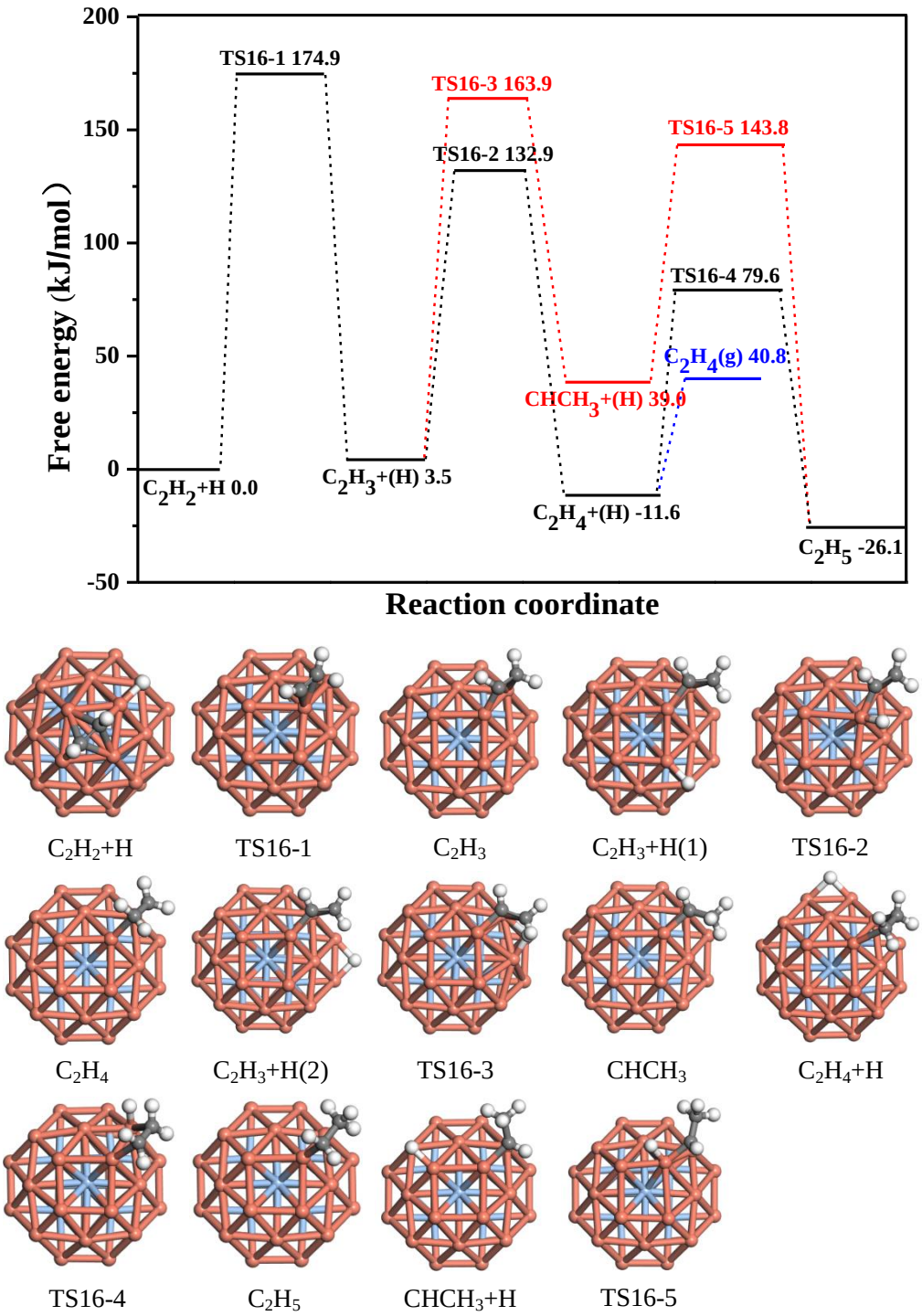

Figure S12 The structures of initial states, transition states, final states of three possible routes involving in C_2H_2 selective hydrogenation on $Ag_6@Cu_{32}$ cluster.

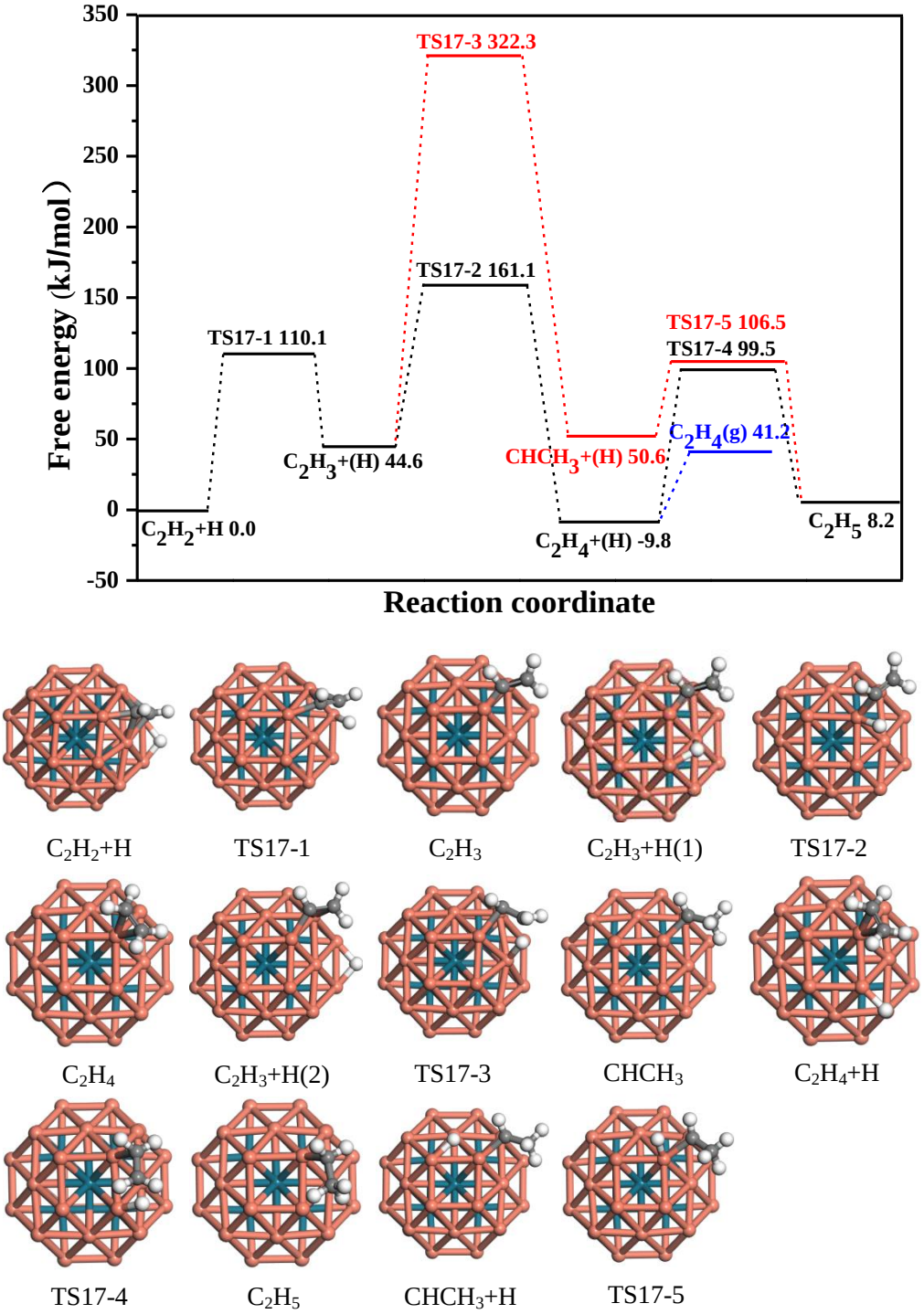

Figure S13 The structures of initial states, transition states, final states of three possible routes involving in C_2H_2 selective hydrogenation on $Pd_6@Cu_{32}$ cluster.

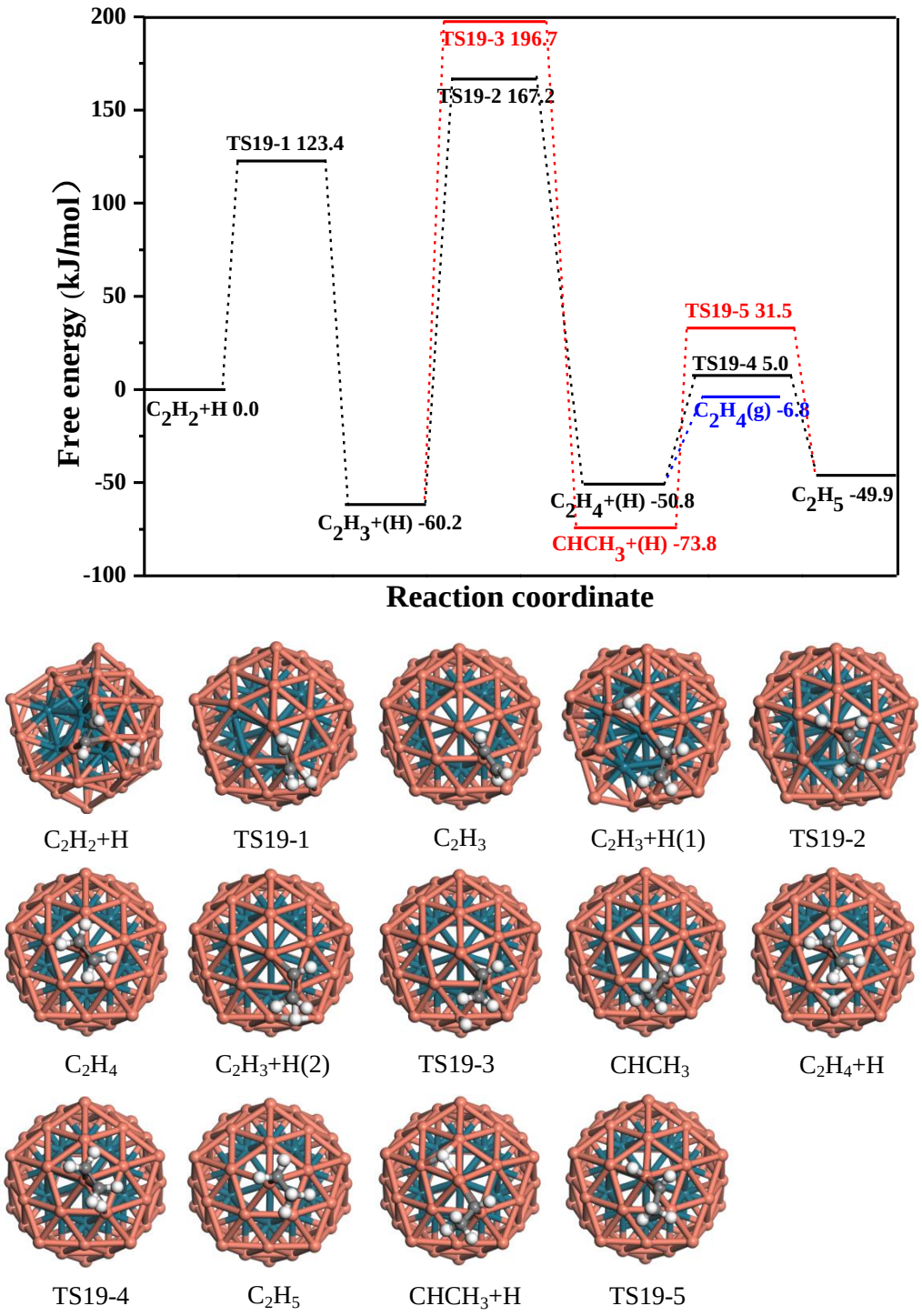

Figure S14 The structures of initial states, transition states, final states of three possible routes involving in C_2H_2 selective hydrogenation on $Cu_{13}@Pd_{42}$ cluster.

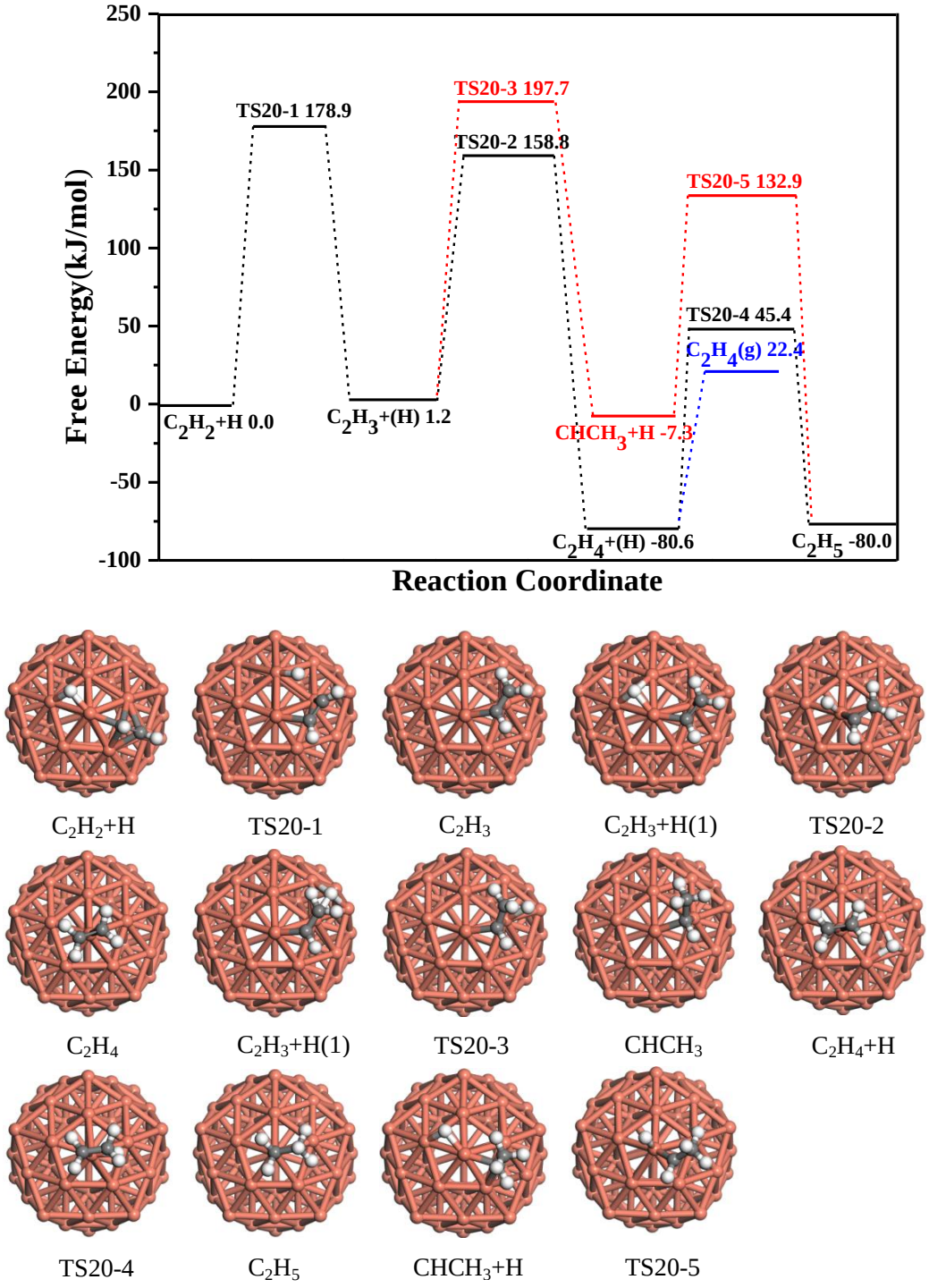

Figure S15 The structures of initial states, transition states, final states of three possible routes involving in C_2H_2 selective hydrogenation on single Cu_{55} cluster.

4. Two-step model of C_2H_4 formation over different sizes of M@Pd(M=Au, Ag and Cu) and M@Cu(M=Au, Ag and Pd) nanoclusters

Previous studies[11-13] have proposed a two-step model to describe catalytic processes on solid surfaces, which can be regard as:

$$R_g+*\rightleftharpoons I_{ad} \qquad I_{ad}\rightleftharpoons P_g+* \tag{1}$$

Where R_g and P_g are the gas-phase reactants and products, I_{ad} is the adsorption state of the intermediates. In the present study, this model has been adopted to measure the activity of C_2H_2 hydrogenation. In this case, R_g and P_g correspond to $C_2H_2(g)+H_2(g)$ and $C_2H_4(g)$, respectively. The energy profile of the two step model of C_2H_2 hydrogenation is shown in Figure S16.

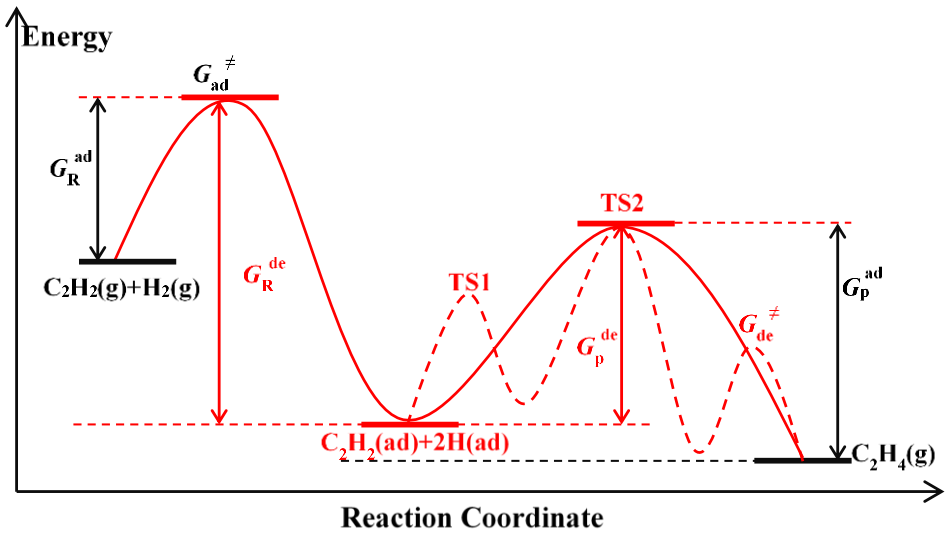

Figure S16 Two-step model, namely the adsorption of the reactants ($C_2H_2+H_2$) and associative desorption of the products (C_2H_4) of C_2H_2 hydrogenation to form C_2H_4 process. G_R^{ad} and G_R^{de} are the free barriers of the adsorption of the reactants and its reverse reaction, respectively. Similarly, G_P^{ad} and G_P^{de} are the free barriers of the adsorption of the products and its reverse reaction, respectively. $G_{ad}^{\neq}$ and $G_{de}^{\neq}$ are the free energy of the transition state for the adsorption of the reactants and the desorption of the products, respectively.

The adsorption rate (r_{ad}) and desorption rate (r_{de}) can be defined as follows:

$$r_{ad} = \frac{k_B T}{h} e^{-\frac{G_R^{ad}}{RT}} \frac{P_R}{P^0} \theta_*(1-z_{ad}) \tag{2}$$

$$r_{de} = \frac{k_B T}{h} e^{-\frac{G_P^{de}}{RT}} \theta_I (1 - z_{de}) \quad (3)$$

Where P_R, P_P, and P^0 are the partial pressures of the reactant, product and the standard pressure, respectively. k_B and h are Boltzmann constant and Planck's constant, respectively. G_R^{ad} and G_P^{de} are the effective free barriers of the reactant adsorption and the product desorption, respectively. z_{ad} and z_{de} are the reversibility of the adsorption and desorption, respectively, which can be expressed as follows:

$$z_{ad} = \frac{P^0 \theta_I}{P_R \theta_* K_{ad}} \quad (4)$$

$$z_{de} = \frac{P_P \theta_*}{P^0 \theta_I K_{de}} \quad (5)$$

Where K_{ad} and K_{de} is the equilibrium constant of the adsorption and desorption processes, respectively. Under the steady state condition, the relationship of $r=r_{ad}=r_{de}$ and $\theta_I + \theta_* = 1$ can be obtained, thus, the reaction rate can be written as follows:

$$r = \frac{k_B T}{h} \frac{(1 - \frac{P_P}{P_R} e^{\frac{\Delta G}{RT}})}{\frac{P^0}{P_R} e^{\frac{G_R^{ad}}{RT}} + \frac{P^0}{P_R} e^{\frac{G_R^{ad} - G_R^{de} + G_P^{de}}{RT}} + e^{\frac{G_P^{de}}{RT}} + \frac{P_P}{P_R} e^{\frac{\Delta G + G_R^{de}}{RT}}} \quad (6)$$

ΔG is the free energy change of the overall reaction, the obtained value from DFT calculations is -184.1 kJ mol^{-1}.

For C_2H_2 hydrogenation on the different sizes of M@Pd and M@Cu core-shell catalysts, it is reasonable to assume that the process is controlled by desorption rate but not the adsorption rate. Thus, the adsorption process reaches quasi-equilibrium and z_{ad} is close to 1. Thus, the reaction rate can be abbreviated as the Eq. (7), in which the coverage terms of adsorbed species involving in the selective hydrogenation of C_2H_2 have been expressed as the energetic terms.

$$r = \frac{k_B T}{h} \frac{(1 - \frac{P_P}{P_R} e^{\frac{\Delta G}{RT}})}{\frac{P^0}{P_R} e^{\frac{G_R^{ad} - G_R^{de} + G_P^{de}}{RT}} + e^{\frac{G_P^{de}}{RT}}} \quad (7)$$

Where ΔG is the activation free energy of overall C_2H_2 hydrogenation to C_2H_4 reaction; G_P^{de} is the free energy of product desorption. P^0, P_R, and P_P are the standard pressure, partial pressures of reactant and product, respectively. T, k_B, h, R are the temperature, Boltzmann constant, Planck's constant, and universal gas constant, respectively. G_R^{ad} and G_R^{de} are the free energies of reactant adsorption and desorption, respectively. All free energies in this study are obtained at 520 K.

References

(1) Perdew, J. P.; Wang, Y. Accurate and Simple Analytic Representation of the Electron-Gas Correlation Energy. *Phys. Rev. B* **1992**, *45*, 13244–13249.

(2) Perdew, J. P.; Burke, K.; Ernzerhof, M. Generalized Gradient Approximation Made Simple. *Phys. Rev. Lett.* **1996**, *77*, 3865–3868.

(3) Delley, B. From Molecules to Solids with the DMol^3 Approach. *J. Chem. Phys*. **2000**, *113*, 7756–7764.

(4) Delley, B. Ground-State Enthalpies: Evaluation of Electronic Structure Approaches with Emphasis on the Density Functional Method. *J. Phys. Chem. A* **2006**, *110*, 13632–13639.

(5) Basiuk, V. A.; Borys-Sosa, P. A. Interaction of Au Atom with Fullerene C60: Performance of DFT Functionals Incorporated Into the DMol^3 Module. *J. Comput. Theor. Nanosci*. **2013**, *10*, 1–6.

(6) Koelling, D. D.; Harmon, B. N. A Technique for Relativistic Spin-Polarised Calculations. *J. Phys. C: Solid. State. Phys.* **1977**, *10*, 3107–3114.

(7) Douglas, M.; Kroll, N. M. Quantum Electrodynamical Corrections to the Fine Structure of Helium. *Ann. Phys.* **1974**, *82*, 89–155.

(8) Delley, B. Hardness Conserving Semilocal Pseudopotentials. *Phys. Rev. B* **2002**, *66*, 155125−155133.

(9) Dolg, M.; Wedig, U.; Stoll, H.; Preuss, H. Energy-Adjusted Abinitio Pseudopotentials for the First row Transition Elements. *J. Chem. Phys.* **1987**, *86*, 866−872.

(10) Bergner, A.; Dolg, M.; Kuechle, W.; Stoll, H.; Preuss, H. Ab Initio Energy-Adjusted Pseudopotentials for Elements of Groups 13–17. *Mol. Phys.* **1993**, *80*, 1431−1441.

(11) Varejão, C. G. Influence of Surface Structures, Subsurface Carbon and Hydrogen, and Surface Alloying on the Activity and Selectivity of Acetylene Hydrogenation on Pd Surfaces: A Density Functional Theory Study. *J. Catal*. **2013**, *305*, 264–276.

(12) Cheng, J.; Hu, P.; Ellis, P.; French, S.; Kelly, G.; Lok, C. M. Brønsted-Evans-Polanyi Relation of Multistep Reactions and Vlcano Curve in Heterogeneous Catalysis. *J. Phys. Chem. C* **2008**, *112*, 1308–1311.

(13) Cheng, J.; Hu, P. Theory of the Kinetics of Chemical Potentials in Heterogeneous Catalysis. *Angew. Chem. Int. Ed*. **2011**, *50*, 7650–7654.